

Application of soft computing techniques for modeling and analysis of MRR and taper in laser machining process as well as weld strength and weld width in laser welding process

Mansour Aminian · Reza Teimouri

Published online: 4 May 2014
© Springer-Verlag Berlin Heidelberg 2014

Abstract The present work deals with modeling and analysis of laser material processing technologies which were commonly used in the recent past. The characteristics of laser machining and laser welding have been determined using response surface method (RSM), artificial neural network (ANN) and adaptive neuro-fuzzy inference system (ANFIS). For each process, an experimental setup was designed and site-conducted using central composite design (CCD). Then their performance measures (responses) have been modeled and predicted based on RSM, ANN and ANFIS. The accuracies of developed models were compared with each other based on prediction error percent. The effects of each process's parameters on its performance measures were analyzed based on graphs which were plotted using the most accurate model. Results indicated that for both types of laser manufacturing processes, the ANFIS method predicted more accurate results. Following ANFIS, ANN and RSM showed almost precise prediction in modeling of performance measures. Hence, the ANFIS technique can be applied for modeling of laser material processing technologies.

Keywords Laser cutting · Laser welding · Modeling · RSM · ANN · ANFIS

Communicated by A. Lotfi.

M. Aminian
Department of Mechanical Engineering, Faculty of Engineering,
University of Tabriz, Tabriz, Iran

R. Teimouri (✉)
Department of Mechanical Engineering,
Babol University of Technology, Babol, Iran
e-mail: reza_teimoori@yahoo.com

1 Introduction

Laser light differs from ordinary light because it has the photons of same frequency, wavelength and phase. Thus, unlike ordinary light, laser beams are highly directional and have high power density and better focusing characteristics (Chryssolouris 1991). These unique characteristics of laser beam are useful in processing of materials. The laser beams are widely used for machining and other manufacturing processes such as, cutting, drilling, micromachining, marking, welding, sintering, surfacing and heat treatment.

The main factors which contribute to laser manufacturing processes are laser power, laser scanning speed, laser pulse duration, laser pulse diameter and laser focusing distance. Due to wide range of processing factors, development of the predictive models for correlation relationships between processes parameters and their performance measures is a major challenge. For this purpose, in recent years, researchers have focused on the modeling of processes based on data obtained through experimental observations. In this case, statistical analysis such as response surface methodology (RSM) is used most commonly to correlate empirical relationship between process factors and responses. Choudhury and Shirley (2010) applied RSM for analyzing effect of laser power, cutting speed and air pressure on heat affected zone thickness, surface roughness and dimensional accuracy while laser cutting of three types of polymeric materials. Dhupal et al. (2009) used five factors–five levels central composite design for evaluating the effect of laser turning process parameters such as lamp current, pulse frequency, pulse width, cutting speed and assist gas pressure on the quality of the laser turned micro-grooves. Kuar et al. (2006) utilized RSM and central composite design for finding optimal settings of lamp current, pulse frequency, pulse width and air pressure for minimizing the thickness of heat affected zone and taper-

ing of micro-drilled holes. Ghosal and Manna (2013) applied RSM for modeling and optimization of laser machining of Al/Al₂O₃ metal matrix composite. They designed 32 experiments based on rotatable central composite design to investigate effects of laser power, modulation frequency, gas pressure, wait time, pulse width on the material removal rate and tapering of grooves. The literatures previously stated were reviewed and surveyed for application of RSM on laser machining processes. This method was also used for analyzing other alternatives of laser manufacturing processes. For example, Acherjee et al. (2009) used the response surface method for analyzing effect of laser power, welding speed, standoff distance and clamp pressure on welding strength and welding width of welding processes included thermoplastic materials. In another attempt, Acherjee et al. (2012) applied RSM along with desirability approach to find optimal settings of laser power, scanning speed, and focusing distance and clamp pressure for simultaneous optimization of Lap-shear strength and weld-seam width of dissimilar materials. Also, the RSM method is most commonly used for modeling of bead geometry of laser cladding process. Onwubolu et al. (2007) utilized the RSM for predicting clad angle, clad height and clad width of surfaces which were coated by laser cladding process. Sun and Hao (2012) combined RSM with desirability approach for modeling and optimization of dimensional accuracy of melt pool profile.

Predictive models based on artificial intelligence are secondary tools that use data generated through experiments for modeling of manufacturing processes characteristics. Artificial neural network, fuzzy logic and neuro-fuzzy system are widely used for modeling of manufacturing processes. Teimouri et al. (2012) used various types of neural networks for modeling spring-back in V-bending process. Teimouri and Baseri (2012b) applied back-propagation neural network (BPNN) along with radial basis function neural network for predicting material removal rate and surface roughness of dry EDM process. Additionally, they applied neural network and neuro-fuzzy inference system for modeling of surface roughness change while magnetic abrasive finishing of hardened AISI 52100 steel (Teimouri and Baseri 2012a). Shayan et al. (2013) also used the neural network and RSM to estimate cutting velocity, surface roughness and over cut of dry wire cut machining of cemented tungsten carbide. In another attempt Teimouri and Baseri (2013a) applied fuzzy logic for forward and backward prediction of friction stir welding process parameters. According to reviewed literatures, it can be inferred that although the predictive models based artificial intelligence have been extensively used for modeling various types of manufacturing processes, there are not many of publications that applied these methods for modeling of laser manufacturing process.

The aim of the present work is to find appropriate method for modeling the characteristics of laser machining and laser

welding processes. For this purpose, the experimental observations of literatures (Ghosal and Manna 2013) and (Acherjee et al. 2012) are used. For each process the RSM, ANN and ANFIS are applied separately, and the accuracies of developed models are compared with each other according to values of prediction error percent (PEP). Afterward the effects of process parameters on performance measures of each process are analyzed using graphs which are obtained through the most accurate method. The present works consists of five main sections. After introduction, in Sect. 2, the methodologies of RSM, ANN and ANFIS are described based on existing references. The Sect. 3 is allocated to the experimentations including experimental setup, experimental material and experimental designs for each process. The Sect. 4 includes obtained results and related discussions. Finally, section five will summarize the results and explain conclusions. The present work deals with application of statistical method like RSM, and intelligent methods like ANN and ANFIS in laser manufacturing processes. The laser manufacturing processes are really expensive; therefore, application of these methods is beneficial to reduce the cost of the process by preventing from conducting huge number of experiments.

2 Methodologies

2.1 Response surface methodology (RSM)

Response surface methodology (RSM) is a collection of mathematical and statistical techniques useful for analyzing problems in which several independent variables influence a dependent variable or response, and the goal is to optimize this response. In many experimental conditions, it is possible to represent independent factors in quantitative form as given in following equation. Then these factors can be thought of as having a functional relationship with a response as follows:

$$Y = \phi(X_1, X_2, \dots, X_k) \pm e_r \quad (1)$$

This represents the relation between response Y and X_1, X_2, \dots, X_k of k quantitative factors. The function Φ is called response surface or response function. The residual e_r measures the experimental errors. For a given set of independent variables, a characteristic surface is responded. When the mathematical form of Φ is not known, it can be approximated satisfactorily within the experimental region by a polynomial.

In this investigation, RSM was applied to develop mathematical models in the form of multiple regression equations for the quantitative characteristics of laser machining and laser welding processes. In applying the RSM, the dependent variable is viewed as a surface to which a mathematical

model is fitted. For the development of regression equations related to various quality characteristics of laser machining and laser welding processes, the second order response surface was assumed to be:

$$Y = b_0 + \sum_{i=1}^k b_i X_{iu} + \sum_{i=1}^k b_{ii} X_{iu}^2 + \sum_{i,j=1}^k b_{ij} X_{iu} X_{ju} \quad (2)$$

where Y is the response; b_0, b_i, b_{ii} and b_{ij} are the coefficients; X_{iu} is the variable; u is the experiment number (1–31 for laser machining or 1–30 for laser welding); k is the factor number (1–5 for laser machining or 1–4 for laser welding); X_{iu}^2 is the second order term of variable and $X_{iu} \times X_{ju}$ are the interaction terms.

Further clarifications about details of RSM and its implementation can be found in literature (Shayan et al. 2013).

In the present study application of RSM is analyzed on laser machining process and laser welding process. To better recognize the developed model of each process, the parameters of laser machining process are characterized by x_i and parameters of laser welding process is characterized by y_i .

2.2 Back-propagation neural network (BPNN)

Use of neural network is popular in telecommunication, signal processing, pattern recognition, prediction, automated control and economical analysis. Back-propagation neural network has been adopted in literatures due to its accuracy and fast response. The BP structure consists of an input layer, some hidden layers and an output layer. In this structure neurons are connected to each other by some weighted links. The information from input layer is mapped to output layer through one or more hidden layers. The relationship between input–output of a single node can be written as following equation.

$$a_k = f \left(\sum_{i=1} W_{ki} p_i + b_k \right) \quad (3)$$

where a_k is the value of node output, W_{ki} is the weight connection between inputs and nodes, p_i is the output of previous nodes in their hidden layer, and b_k is the bias value of the node and finally f is activation function. Generally the activation functions selected for hidden layers are log-sigmoid. The linear function is recommended for the output layer.

Modeling and prediction of specified process characteristics by BPNN consist of two main stages, namely, training and testing. In the training stage, a network is trained by using collection of experimental data (about 80 %) and the network parameters such as number and size of hidden layer(s), type of transfer functions and network learning rate are set. In the testing stage, the trained network is tested by the remaining

data sets (20 % of data) and its performance is checked based on value of mean absolute error (MAE) described by Eq. (4). Also, due to small number of experiments (only 31 experiments for laser machining process and 30 experiments for laser welding process those includes 6 replications at center point), the cross-validation is neglected.

$$MAE = \frac{1}{T} \sum_{i=1}^T |t_i - a_i| \quad (4)$$

where T is the number of testing data, t_i is the target value and a_i is ANN modeled value.

The training and testing of a network are repeated under various network architectures, various transfer functions and different learning rates until the network reaches the lowest value of MAE according to trial and error methodology. For further information about implementation of BPNN, it is suggested that interested readers read literatures (Teimouri et al. 2012; Teimouri and Baseri 2012a, b; Shayan et al. 2013) which were written by corresponding author.

2.3 Adaptive neuro-fuzzy inference system (ANFIS)

An ANFIS is a hybrid predictive model which uses both neural network and fuzzy logic to generate mapping relationship between inputs and outputs (Teimouri and Baseri 2013b). The structure of this model consists of five layers with each layer being constructed of several nodes. Similar to a neural network, in an ANFIS structure the inputs of each layer are gained by the nodes from previous layer. The ANFIS network includes m inputs ($X_1 \dots X_m$), each one consisting of n membership functions (MFs). Moreover, a layer with R fuzzy rules and also an output layer are contributed to construction of this model. The number of nodes in the first layer can be calculated by the product of m as number of inputs and n as number MFs ($N = m \cdot n$). Number of nodes in other layers (layer 2–4) relates to number of fuzzy rules (R).

Like a neural network, modeling of specified process characteristics by ANFIS consists of two main stages of training and testing. Here, the number of membership functions (MFs) and types of MFs are the main network parameters and play important roles in prediction by ANFIS. Like a neural network, in modeling by ANFIS, the training and testing are repeated under various network architectures (number of MFs) and various types of MFs until the network reaches to lowest value of RMSE according to the following equation:

$$RMSE = \sqrt{\frac{1}{M} \sum_{z=1}^M (S_z - Y_z)^2} \quad (5)$$

where M is number of data in testing (in this work $M = 31$ and 30 for laser machining and laser welding, respectively)

S_z is the real value of a given output obtained by experiments and Y_z is the value of predicted output by developed models.

For further information about implementation of the ANFIS, the interested readers can read reference (Teimouri and Baseri 2013b; Teimouri et al. 2013; Babajanzade-Roshan et al. 2013; Kashiry Fard et al. 2013).

In present work, due to small number of experiments (only 31 experiments for laser machining process and 30 experiments for laser welding process those includes 6 replications at center point), the cross-validation of ANN and ANFIS is performed by splitting experimental data sets of Tables 2 and 4 in five folds. In other words, training/testing of a network is applied for five times under various training/testing data configurations (Teimouri and Baseri 2013b). Appendixes A and B presents data sets with theirs corresponding five folds those are used for training/testing of laser machining and laser welding, respectively. In these tables (i.e. "Appendixes A and B") data sets which symbolized by "*" are used for testing of network and the other non-symbolized sets are utilized for training.

In the present study the MAE and RMSE are used to find appropriate structure of ANN and ANFIS, respectively. They are used according the default of neural network toolbox and ANFIS Toolbox in MATLAB software. Also, to compare accuracy of developed models, another comparative tool, namely, prediction error percent (PEP) is defined as percentage of deviation of predicted value from absolute value.

3 Experimentations

In this section experimental setup, materials and procedures are explained for laser drilling and laser welding, separately. The specifications of each experiment are described as follows:

3.1 Experimentations of laser machining process

For this process, an ytterbium laser machine equipped with CNC attachment was used to conduct experiments. The workpiece material is from Al/Al₂O₃ metal matrix composite that is extensively used in air plane industry. Due to high hardness and corrosion resistance of this metal it is categorized as difficult-to-cut material. The process predominant factors were laser power, modulation frequency, gas pressure, wait time and pulse width. The ranges of factors were selected based on machine quality and laboratory experiments. The main responses of the process were material removal rate (MRR) and phenomenon of tapering (Ta). The MRR is calculated by dividing workpiece mass loss to machining time. Also, the taper of machined holes is calculated by following equation.

Table 1 Laser machining predominant factors and their levels

Process factors	Symbols	Units	Levels				
			-2	-1	0	1	2
Laser power	x_1	W	400	500	700	900	1,000
Modulation frequency	x_2	Hz	600	700	800	900	1,000
Gas pressure	x_3	bar	15	16	17	18	20
Wait time	x_4	s	0.1	0.15	0.2	0.25	0.3
Pulse width	x_5	%	75	80	90	95	100

$$Ta(\text{rad}) = \left[\tan^{-1}(D - d)/2t \right] \quad (6)$$

where D is measured diameter at top of the machined hole, d is the measured diameter at bottom of the machined hole and t is the workpiece thickness.

Table 1 presents the process factors and their levels. The rotatable central composite DOE technique was used for design and conduction of experiments. Table 2 presents the experimental design matrix and obtained values of material removal rate and tapering of machined holes. Further clarifications about experimentations of laser drilling process can be found in literature (Ghosal and Manna 2013).

3.2 Experimentations of laser transmission welding process

For this process, experimental observations are performed with a continuous wave diode laser system. The system installation consists of a 30 W coherent fibered array package (FAP) diode laser with a 3-axes CNC work table. The diode laser is operated at 809.4 nm wavelength and the focal length used is 13 mm. The workpiece materials for joining dissimilar polymers are Plexiglass 6N acrylic (PMMA) granules from Evonik Rohm GmbH and Terlurans GP-22 ABS granules from BASF. The predominant factors of this process were laser power, welding speed, standoff distance and clamp pressure. Table 3 presents process factors and their levels. The experiments were designed and conducted based on four factors-five levels central composite design to study effect of process factors on weld strength and weld width. The weld strength is calculated by a microprocessor controlled Instron universal testing machine with an accuracy of 70.4 % of rated capacity (model: 8801, maximum capacity: 100 kN) that is suitable for lap-shear pull test of welded specimens. For measuring weld seam width, a STM6 microscope offers high performance three axis measurements of parts, with sub-micron precision. Inbuilt LED illuminator is used for reflected coaxial illumination during measurements. Table 4 presents design matrix and experimental results for laser transmission welding process.

Table 2 Design matrix and experimental results for laser drilling processes

No.	Factors					Responses	
	x_1	x_2	x_3	x_4	x_5	MRR (g/s)	Taper (rad)
1	-1	-1	-1	-1	1	0.2404	0.0040
2	1	-1	-1	-1	-1	0.1701	0.0043
3	-1	1	-1	-1	-1	0.2357	0.0049
4	1	1	-1	-1	1	0.3184	0.0040
5	-1	-1	1	-1	-1	0.3126	0.0030
6	1	-1	1	-1	1	0.2988	0.0050
7	-1	1	1	-1	1	0.2272	0.0046
8	1	1	1	-1	-1	0.2272	0.0048
9	-1	-1	-1	1	-1	0.2299	0.0052
10	1	-1	-1	1	1	0.2346	0.0042
11	-1	1	-1	1	1	0.2316	0.0043
12	1	1	-1	1	-1	0.2346	0.0038
13	-1	-1	1	1	1	0.2312	0.0036
14	1	-1	1	1	-1	0.2356	0.0042
15	-1	1	1	1	-1	0.2351	0.0044
16	1	1	1	1	1	0.2332	0.0042
17	-2	0	0	0	0	0.2334	0.0040
18	2	0	0	0	0	0.2363	0.0048
19	0	-2	0	0	0	0.2321	0.0042
20	0	2	0	0	0	0.2330	0.0045
21	0	0	-2	0	0	0.2344	0.0040
22	0	0	2	0	0	0.2355	0.0041
23	0	0	0	-2	0	0.2604	0.0047
24	0	0	0	2	0	0.2324	0.0043
25	0	0	0	0	-2	0.2372	0.0045
26	0	0	0	0	2	0.2381	0.0049
27	0	0	0	0	0	0.2399	0.0046
28	0	0	0	0	0	0.2391	0.0047
29	0	0	0	0	0	0.2416	0.0047
30	0	0	0	0	0	0.2761	0.0044
31	0	0	0	0	0	0.2824	0.0043

Table 3 Laser welding predominant factors and their levels

Process factors	Symbols	Units	Levels				
			-2	-1	0	1	2
Laser power	y_1	W	9	12	15	18	21
Welding speed	y_2	mm/s	4	8	12	16	20
Stand-off-distance	y_3	mm	26	32	38	44	50
Clamp pressure	y_4	MPa	0.9	1.5	2.1	2.7	3.3

For further information about experimentations, it is suggested that interested readers read the experimental section of literature (Acherjee et al. 2012).

4 Results and discussions

In this section, results of soft computing models for prediction of characteristics of laser machining, laser welding and laser cladding processes are presented. For each process, the characteristics are modeled based on RSM (using Design Expert V8 DOE software), ANN (using MATLAB R17 neural network ToolBox) and ANFIS (using MATLAB R17 ANFIS ToolBox). Subsequently, the accuracies of developed models are compared based on PEP. Afterward, the effects of process parameters on performance measures of each process are analyzed based on graphs which were obtained through the most accurate models.

Table 4 Design matrix and experimental results for laser welding process

No.	Factors				Responses	
	y_1	y_2	y_3	y_4	Weld strength (N/mm)	Weld width (mm)
1	-1	-1	-1	-1	38.29	3.19
2	1	-1	-1	-1	31.14	3.43
3	-1	1	-1	-1	45	2.74
4	1	1	-1	-1	46.14	3.14
5	-1	-1	1	-1	62.43	4.51
6	1	-1	1	-1	79.26	5.17
7	-1	1	1	-1	32.57	3.36
8	1	1	1	-1	58.71	4.10
9	-1	-1	-1	1	38.71	3.15
10	1	-1	-1	1	22.14	3.42
11	-1	1	-1	1	55.29	2.74
12	1	1	-1	1	40.43	3.15
13	-1	-1	1	1	65.57	4.92
14	1	-1	1	1	71.71	5.28
15	-1	1	1	1	46.86	3.35
16	1	1	1	1	57.14	4.37
17	-2	0	0	0	55.14	3.26
18	2	0	0	0	65.57	4.31
19	0	-2	0	0	40.57	4.78
20	0	2	0	0	48.29	3.42
21	0	0	-2	0	9.71	2.21
22	0	0	2	0	41.71	4.26
23	0	0	0	-2	63.71	3.81
24	0	0	0	2	62.29	4.14
25	0	0	0	0	63.29	4.08
26	0	0	0	0	65.43	3.91
27	0	0	0	0	64	3.98
28	0	0	0	0	63.57	4.10
29	0	0	0	0	62.14	3.99
30	0	0	0	0	64.57	4.01

4.1 Modeling and analysis of laser machining process characteristics

4.1.1 Modeling of MRR and T_a by RSM

4.1.1.1 Modeling of MRR Based on regression statistics, it was decided to use a second order model with two-factor interaction terms to correlate empirical relationships between process factors and MRR. Also, the analysis of variances (ANOVA) was done for finding significant factors. Table 5 presents ANOVA results for modeling of MRR. The model $\text{Prob} > f$ is lower than 0.05 (i.e. 0.004) that means the model is significant. Also, the value of $\text{Prob} > F$ for term of “lack-of-fit” is much higher than 0.05 (i.e. 0.8184) that means

the “lack of fit” is insignificant. In this table the values of “ $\text{Prob} > F$ ” < 0.0500 indicate model terms are significant and vice versa. Hence the modified model of MRR based on significant factors is presented at following equation:

$$\begin{aligned} \text{MRR} = & 0.24 - 9.192 \times 10^{-3}x_4 + 9.92E \\ & -003x_1x_2 + 0.019x_1x_5 - 0.019x_2x_3 \\ & -0.011x_3x_5 \end{aligned} \quad (7)$$

where x_1 is laser power, x_2 is modulation frequency, x_3 is gas pressure, x_4 is wait time and x_5 is pulse width.

4.1.1.2 Modeling of T_a According to regression statistics, the quadratic model was found to be a suitable model for

Table 5 ANOVA results for MRR

Source	Sum of squares	Degree of freedom	Mean of square	F value	Prob > F	Significance
Model	0.020	15	1.33E-003	4.09	0.004	Significant
x_1	8.9 E-006	1	8.9E-006	0.027	0.8712	Insignificant
x_2	2.94E-006	1	2.94E-006	9E-3	0.9257	Insignificant
x_3	4.84E-004	1	4.84E-004	1.48	0.2415	Insignificant
x_4	2.02E-003	1	2.02E-003	6.20	0.0242	Significant
x_5	7.7E-004	1	7.75E-004	2.37	0.1433	Insignificant
x_1x_2	1.57E-003	1	1.57E-003	4.82	0.0433	Significant
x_1x_3	6.16E-005	1	6.16E-005	0.19	0.6701	Insignificant
x_1x_4	8.41E-006	1	8.41E-006	0.026	0.8746	Insignificant
x_1x_5	5.64E-003	1	5.64E-003	17.23	0.0008	Significant
x_2x_3	5.65E-003	1	5.65E-003	17.28	0.0007	Significant
x_2x_4	1.72E-005	1	1.72E-005	0.053	0.8215	Insignificant
x_2x_5	2.75E-005	1	2.75E-005	0.084	0.7754	Insignificant
x_3x_4	5.85E-004	1	5.85E-004	1.79	0.1997	Insignificant
x_3x_5	1.91E-003	1	1.19E-003	5.84	0.028	Significant
x_4x_5	1.29E-003	1	1.29E-003	3.95	0.0643	Insignificant
Residual	5.23E-003	16	3.27E-004	-	-	-
Lack-of-fit	2.85E-003	11	2.59E-004	0.54	0.8148	Insignificant

prediction of tapering by RSM. The ANOVA results for modeling of tapering have been presented in Table 6. The model Prob > f is lower than 0.05 (i.e. 0.0019) that means the model is significant. Also, the value of Prob > F for term of “lack of fit” is much higher than 0.05 (i.e. 0.2635) that means the “lack-of-fit” is insignificant. In this table values of “Prob > F” <0.0500 indicate model terms are significant and vice versa. Hence the modified model of Ta based on significant factors is presented at following equation:

$$\begin{aligned}
 Ta = & 4.53 \times 10^{-3} - 1.33 \times 10^{-4}x_3^2 \\
 & -2.063 \times 10^{-4}x_1x_2 + 2.93 \times 10^{-4}x_1x_3 \\
 & -1.68 \times 10^{-4}x_4 + 1.81 \times 10^{-4}x_2x_3 \\
 & -1.56 \times 10^{-4}x_2x_4 + 1.68 \times 10^{-4}x_3x_5 \\
 & -1.18 \times 10^{-4}x_4x_5
 \end{aligned} \tag{8}$$

4.1.2 Modeling of MRR and Ta by ANN

In order to train a back-propagation network for modeling of MRR and tapering, of the 31 data sets, 25 were stochastically selected for network training. The remaining six data sets were then tested by the trained network.

As discussed in Sect. 2.2 training and testing of network under various BP-NN topographies are repeated until the lowest value of MAE is obtained. Hence, here, for modeling of MRR and Tapering, various topographies (networks with various hidden layers and different hidden neurons) under various data folds were trained and tested and their MAEs

were calculated based on trial and error method. Table 7 presents the obtained values of MAE for various ANN topography and different folds. It is seen from the Table 7 that a network with topography of 5-10-2 is the most accurate model due to its lowest values of MAEs. Figure 1 indicates comparison of predicted values of testing data which were obtained through BP-NN with real data obtained through experiments regarding fold #3 (i.e. fold with highest MAEs). It can be inferred from this figure that even for worst prediction (regarding fold #3) there is tight agreements between measured and predicted values of testing data. Hence, the 5-10-2 topography was selected as most accurate architecture for modeling of MRR and Ta in modeling of process via ANN.

4.1.3 Modeling of MRR and Ta by ANFIS

For modeling of MRR and Ta by ANFIS, the numbers of 25 data sets from Table 2 were used for training of ANFIS network, and then the trained network was tested by the other six remaining data sets. To implement cross validation on modeling of MRR and taper by ANFIS, five data folds were identified (according to “Appendix A”). Based on trial and error methodology, the ANFIS network has been trained and tested by various types of MFs until the lowest value of RMSE is obtained. While modeling of MRR and Ta by ANFIS, selection of the structures with higher than 2 MFs for each input resulted in overfitting and due to wide range of process factors and levels, the run time was very long. Table 8 indicates the RMSEs which were

Table 6 ANOVA results for tapering

Source	Sum of squares	Degree of freedom	Means of squares	F value	Prob > F	Significance
Model	5.53E00-6	20	2.7E00-7	6.10	0.0019	Significant
x_1	1.83E00-7	1	1.83E00-7	4.05	0.0694	Insignificant
x_2	1.83E00-7	1	1.83E00-7	4.05	0.0694	Insignificant
x_3	2.04E00-8	1	2.05E00-8	0.45	0.5163	Insignificant
x_4	9.37E00-8	1	9.37E00-8	2.07	0.1785	Insignificant
x_5	4.16E00-10	1	4.16E00-10	9.17E-3	0.9254	Insignificant
x_1^2	6.06E00-8	1	6E-008	1.33	0.2724	Insignificant
x_2^2	9.85E00-8	1	9.85E-008	2.17	0.1687	Insignificant
x_3^2	5.185E00-7	1	5.18E-007	11.42	0.0061	Significant
x_4^2	1.22E00-8	1	1.22E-008	0.27	0.6134	Insignificant
x_5^2	2.56E00-8	1	2.56E-008	0.56	0.4684	Insignificant
x_1x_2	6.8E00-7	1	6.8E-007	14.99	0.0026	Significant
x_1x_3	1.38E00-6	1	1.38E-006	30.41	0.0002	Significant
x_1x_4	4.55E00-7	1	4.55E-007	10.04	0.0090	Significant
x_1x_5	1.05E00-7	1	1.05E-007	2.33	0.1554	Insignificant
x_2x_3	5.2E00-7	1	5.25E-007	11.58	0.0059	Significant
x_2x_4	3.9E00-7	1	3.9E-007	8.6	0.0136	Significant
x_2x_5	5.06E00-8	1	5.06E-008	1.12	0.3136	Insignificant
x_3x_4	1.056E00-7	1	1.05E-007	2.33	0.1554	Insignificant
x_3x_5	4.55E00-7	1	4.55E-007	10.04	0.0090	Significant
x_4x_5	2.25E00-7	1	2.25E-007	4.97	0.0476	Significant
Residual	5E00-7	11	4.54E-008	-	-	-
Lack-of-fit	3.5E00-7	6	5.85E-008	0.97	0.2635	Insignificant

Table 7 Obtained MAE for various neural network topographies under various data folds for MRR and Taper

Structure	Mean absolute error (MAE)					
	Fold #1	Fold #2	Fold #3	Fold #4	Fold #5	Average
MRR						
5-7-2	0.1652	0.1524	0.1632	0.1391	0.1362	0.1512
5-8-2	0.1431	0.1471	0.1488	0.1265	0.1287	0.1388
5-9-2	0.1319	0.1202	0.1362	0.1183	0.1165	0.1246
5-10-2	0.1121	0.1087	0.1142	0.1021	0.1052	0.1084
5-11-2	0.1322	0.1232	0.1298	0.1249	0.1324	0.1284
5-12-2	0.1541	0.1397	0.1467	0.1578	0.1752	0.1548
Taper						
5-7-2	0.0015	0.0019	0.0017	0.0018	0.0014	0.00166
5-8-2	0.0011	0.0013	0.0017	0.0014	0.0012	0.00134
5-9-2	0.0008	0.0010	0.0015	0.0011	0.0008	0.00104
5-10-2	0.0006	0.0008	0.0011	0.0007	0.0005	0.00074
5-11-2	0.0013	0.0012	0.0018	0.0010	0.0009	0.00124
5-12-2	0.0018	0.0018	0.0020	0.0015	0.0013	0.00168

The best structure regarding lowest prediction error are in bold

obtained through modeling of MRR and Ta under various types MFs and different data folds while the structure is 2-2-2-2-2. It can be inferred from this table that for both MRR and Ta the ANFIS network with triangular types of MFs guarantees lowest RMSE. Figure 2 shows the agree-

ment between measured values of MRR and Ta for testing under data fold #3. (i.e. highest RMSEs). It can be inferred from this figure that the developed ANFIS model has superiority in prediction of laser machining process even for the worst prediction.

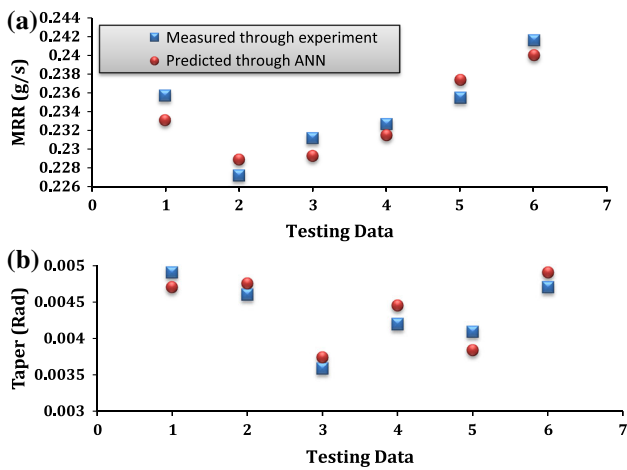


Fig. 1 Comparison of measured and 5-10-2 ANN predicted values of testing data for **a** MRR **b** Ta for fold #3

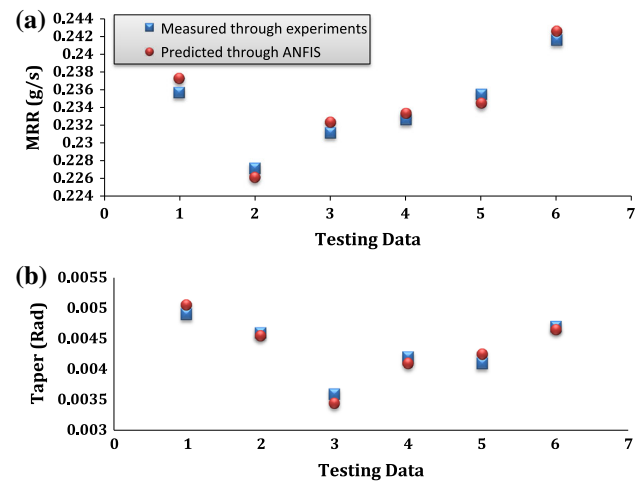


Fig. 2 Comparison of measured and ANFIS predicted values of testing data for **a** MRR **b** Ta for fold #3

4.1.4 Comparison accuracies of developed models

To compare the accuracies of a developed model, the prediction error percentage (PEP) is defined as follows:

$$PEP = \frac{1}{n} \sum_{i=1}^n \frac{|a_i - y_i|}{a_i} \tag{9}$$

where a_i is the measured value obtained by experiments and y_i is the predicted value by the developed RSM, ANN and ANFIS models.

Figure 3a, b indicates graph of PEP for modeling of MRR and Ta by RSM, ANN and ANFIS, respectively. It can be seen from the figure that the developed ANFIS outperforms ANN and in modeling of MRR and Ta due to lowest values of PEP almost in all 31 data sets.

The main reason for outperforming of ANFIS than ANN and RSM, is to regard inputs and outputs in both cases of crisp and linguistic data collections due to contribution of neural network and fuzzy logic, respectively. Hence, for a

complex process such as laser machining, this method can approximate the variations as a powerful artificial intelligence method. Following the ANFIS model, the neural network has outperformed the RSM. This is due to intelligent nature of neural network that leads to more precise prediction rather than statistical method such as RSM.

4.1.5 Effect of laser machining parameters on MRR and Ta based on developed ANFIS model

As it was resulted in previous section, the ANFIS was selected as the most accurate model for prediction both MRR and Ta. Hence, the developed ANFIS model can be used for analyzing effects of laser machining process parameters on MRR and Ta. 3D plots of ANFIS surfaces were drawn and the parameter effects have been analyzed as follows.

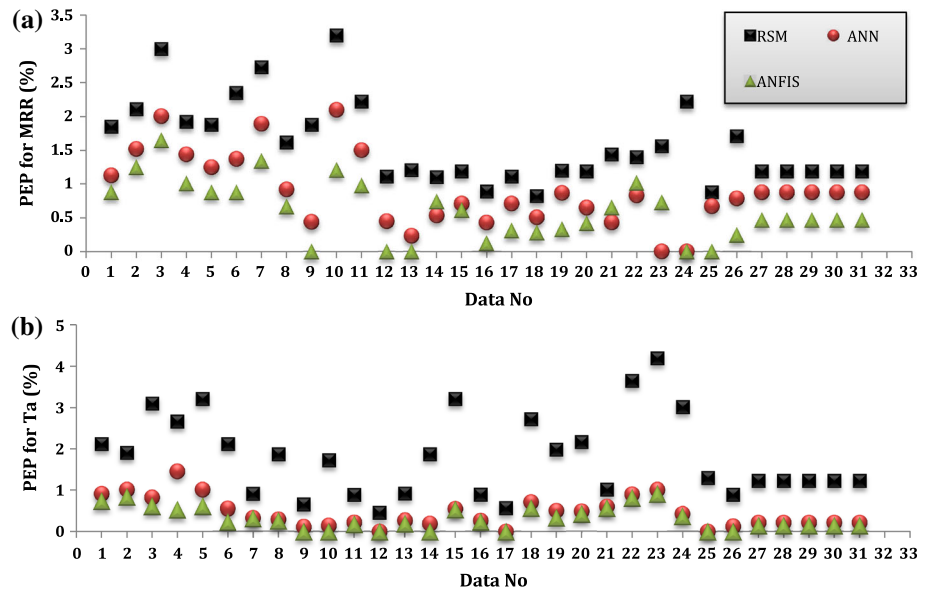
4.1.5.1 Effects of machining parameters on MRR Figure 4a–c indicates interaction effects of process parameters on

Table 8 Obtained RMSEs for various ANFIS MFs under various data folds for MRR and taper

Structure	Root mean square error (RMSE)					
	Fold #1	Fold #2	Fold #3	Fold #4	Fold #5	Average
MRR						
Triangle	0.0741	0.0773	0.0813	0.0621	0.0701	0.07298
Trapezoid	0.2311	0.1982	0.1725	0.1982	0.2311	0.20676
Generalized bell	0.1432	0.1477	0.1566	0.1322	0.1653	0.149
Gaussian	0.1139	0.1282	0.1324	0.1021	0.1174	0.118
Taper						
Triangle	0.0002	0.0003	0.0003	0.0001	0.0002	0.00022
Trapezoid	0.0010	0.0008	0.0009	0.0011	0.0008	0.00074
Generalized bell	0.0005	0.0007	0.0006	0.0006	0.0007	0.00062
Gaussian	0.0004	0.0004	0.0006	0.0007	0.0005	0.00052

The best structure regarding lowest prediction error are in bold

Fig. 3 PEP for modeling of **a** MRR and **b** Ta by RSM, ANN and ANFIS



material removal rate based on surfaces which were plotted by developed ANFIS models. For increasing productivity of the process, it is necessary for the MRR to increase. Hence maximal MRR is desirable.

Figure 4a demonstrates interaction effect of laser power and modulation frequency on MRR. For drawing of this plot the other factors such as assisted gas pressure, wait time and pulse width are kept constant at their center levels (e.g. 17 bar, 0.2 s and 90 % respectively). According to this figure, it is seen that the combination of high laser power and high laser modulation frequency results in a higher MRR. By the increasing laser power a greater amount of thermal energy is transferred to the workpiece. Hence, more material is removed and MRR increases at high laser power. Alternatively, at high laser modulation frequency the thermal energy is transferred to the workpiece for much more time within a specified machining time. Therefore, the combination of high laser power and high modulation frequency lead to high material removal rate.

Figure 4b illustrates interaction effects of wait time and gas pressure. For drawing of this plot the other factors such as laser power, modulation frequency, and pulse width are kept constant at their center levels (e.g. 500 W, 800 Hz and 85 % respectively). It can be seen from the figure that irrespective to wait time, the material removal rate firstly increases by increasing in gas pressure, then by further increase in gas pressure the MRR decreases slightly. When the gas pressure increases (from initial level to a specified value), the jet of high flow nitrogen gas facilitates removal of molten material from workpiece. However, further increasing gas pressure, further flow of gas is injected into the machining gap and due to the cooling nature of nitrogen it may lead to reduction of thermal energy which is transferred to

workpiece. On the other hand it is seen from the figure that irrespective to the gas pressure, by increasing wait time the material removal rate increases correspondingly, then by further increasing laser wait time the MRR decreases gradually. While the wait time increases from 0.1 to 0.15–0.2 s, the MRR increases accordingly due to providing enough relaxing time for removing molten metal from machined holes. However by further increasing wait time from 0.2 to 0.3 s, the material removal rate decreases correspondingly, due to increasing in non-cutting time. In other word, no material is removed while the wait time increases from 0.2 to 0.3 s.

Figure 4c presents interaction effect of laser power and pulse width on MRR. For drawing of this plot the other factors such as modulation frequency, assisted gas pressure and wait time are kept constant at their center levels (e.g. 800 Hz, 17 bars and 0.2 s respectively). It can be seen from this figure that high pulse power and high pulse width combination result in a high MRR. In this case, it can be discussed that greater thermal energy transfer to the workpiece results from a wider pulse area. Hence, it can damage more area and remove more material. Therefore, the MRR is high while high laser power and high pulse width are selected.

4.1.5.2 Effect of machining parameters on Ta Figure 5a–c illustrates interaction effects of process parameters on taper phenomenon of machined hole based on surfaces which were plotted by a developed ANFIS model. The lower value of taper implies high product quality and high accuracy. Therefore, the minimal taper is desirable.

Figure 5a demonstrates interaction effects of laser power and modulation frequency on taper of machined hole. For drawing of this plot the other factors such as assisted gas pressure, wait time, and pulse width are kept constant at their

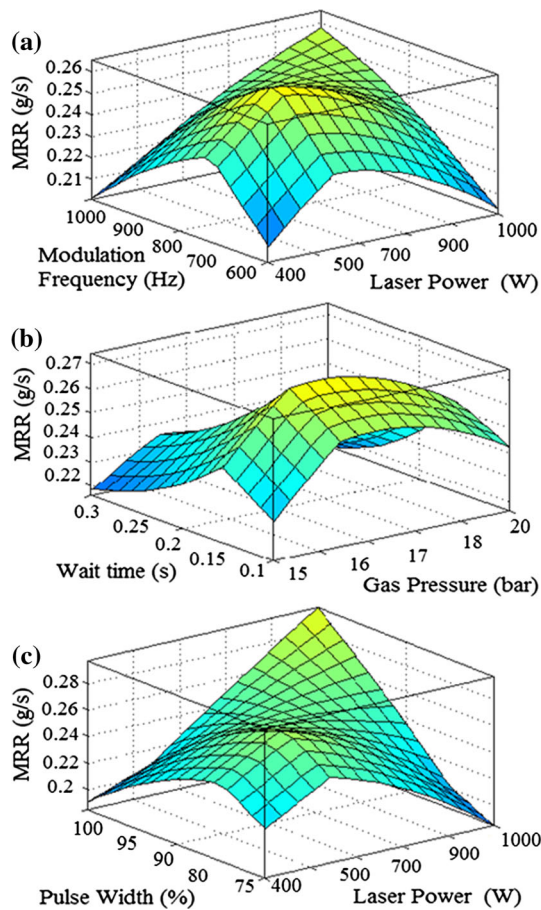


Fig. 4 ANFIS surfaces for interaction effects of parameters on MRR. **a** Interaction of laser power and modulation frequency. **b** Interaction of gas pressure and wait time. **c** Interaction of laser power and pulse width

center levels (e.g. 17 bars, 0.2 s and 90 % respectively). The figure shows that a low laser power and low modulation frequency combination results in low taper. On one hand, low laser power generates lower thermal energy, as a result top surface of work sample where the laser beam is focused, get melted and vaporized slowly and low volume of material is removed from the top surface during penetration into the remaining thickness, which produces low taper. On the other hand, at very low modulation frequency, the laser energy is relatively high, but the time between two successive incident beams is more, therefore, material has been removed only from the narrow focusing spot on the top surface of work sample. Due to low assisted gas pressure, narrow localized heating occurred as a result low tapered hole is generated (Kuar et al. 2006).

Figure 5b presents interaction effect of assisted gas pressure and wait time on taper of laser drilled hole. For the drawing of this plot the other factors such as laser power, modulation frequency, and pulse width are kept constant at their center levels (e.g. 700 W, 800 Hz and 90 % respectively). It can be seen from the figure that at low wait time (high thermal

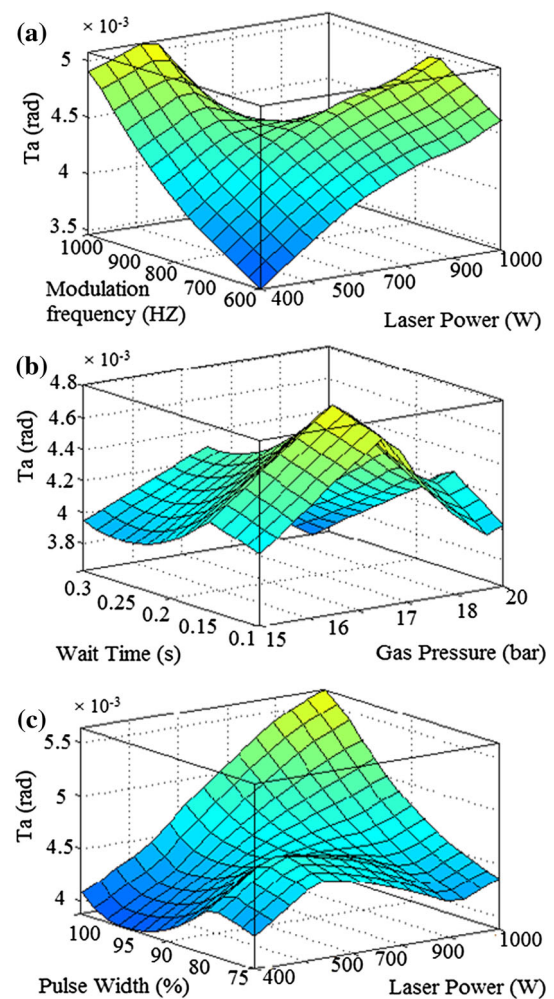


Fig. 5 ANFIS surfaces for interaction effects of parameters on Ta. **a** Interaction of laser power and modulation frequency. **b** Interaction of gas pressure and wait time. **c** Interaction of laser power and pulse width

energy) the taper is increased while the gas pressure increases from its initial level to 17 bars. At low wait time the thermal energy is relatively high and increasing in gas pressure can help the metal removal process. Therefore in such situations more material is removed from the top surface of workpiece and taper increases. By further increase in gas pressure due to cooling characteristic of nitrogen the thermal energy is decreased and it disturbs regular metal removal mechanism and leads to low taper. Also, it is seen from the figure that the wait time has no significant effect on taper. By a precise notation to this figure, it is seen that by increasing the wait time the taper increases due to better removal of molten metals from machining hole and improvement of metal removal process. However, by further increasing the wait time, the taper decreases gradually due to increase in non-cutting time and lower thermal energy within constant machining time.

Figure 5c indicates interaction effects of laser power and pulse width on taper of machined hole. For the drawing of this plot the other factors such as modulation frequency, assisted

Table 9 ANOVA results for welding strength

Source	Sum of squares	Degree of freedom	Means of square	F value	Prob > F	Significance
Model	6,956.97	14	496.93	144.25	<0.0001	Significant
y_1	76.36	1	76.36	22.17	0.0003	Significant
y_2	41.79	1	41.79	12.13	0.0033	Significant
y_3	2,037.07	1	2,037.07	591.35	<0.0001	Significant
y_4	0.090	1	0.090	0.026	0.8737	Insignificant
y_1^2	22.05	1	22.05	6.4	0.0231	Significant
y_2^2	360.99	1	360.99	104.79	<0.0001	Significant
y_3^2	2,505.65	1	2,505.65	727.37	<0.0001	Significant
y_4^2	1.52	1	1.52	0.44	0.5168	Insignificant
y_1y_2	34.37	1	34.37	9.98	0.0065	Significant
y_1y_3	586	1	586	170.11	<0.0001	Significant
y_1y_4	168.81	1	168.81	49	<0.0001	Significant
y_2y_3	1,229.23	1	1,229.23	356.98	<0.0001	Significant
y_2y_4	57.34	1	57.34	16.65	0.001	Significant
y_3y_4	9.47	1	9.47	2.75	0.1181	Insignificant
Residual	51.67	15	3.44	–	–	–
Lack-of-fit	45.32	10	4.53	3.57	0.0865	Insignificant

gas pressure and wait time are kept constant at their center levels (e.g. 800 Hz, 17 bars and 0.2 s respectively). It can be seen from this figure that very high laser power and very high pulse width combination leads to a high value of taper. It is obvious that at high laser power, the high pulse width results in focusing of high thermal energy at wider area. Hence, more volume of material is removed from the top surface of the workpiece and it may lead to high taper. Therefore, to obtain low taper, selection of a lower pulse width and lower laser power are suggested.

4.2 Modeling and analysis of laser welding process characteristics

4.2.1 Modeling of weld strength and weld width by RSM

4.2.1.1 Modeling of weld strength (WS) According to sequential sum of squares and lack-of-fit tests, it was decided to use quadratic model to correlate relationship between laser welding process factors and welding strength. Table 9 presents the ANOVA results for finding significant factors. The model Prob > f is lower than 0.05 (i.e. <0.0001) that means the model is significant. Also, the value of Prob > F for term of “lack-of-fit” is much higher than 0.05 (i.e. 0.0865) that means the “lack of fit” is insignificant. In this table the Values of “Prob > F ” <0.0500 indicate model terms are significant and vice versa. Hence the modified model of WS based on significant factors is presented at following equation:

$$\begin{aligned} WS = & 68.38 + 1.78y_1 - 1.32y_2 \\ & + 9.21y_3 - 0.9y_1^2 - 3.63y_2^2 - 0.956y_3^2 \\ & + 1.47y_1y_2 + 6.05y_1y_3 - 3.25y_1y_4 \\ & - 8.77y_2y_3 + 1.89y_2y_4 \end{aligned} \quad (10)$$

where y_1 is laser power, y_2 is welding speed, y_3 is standoff distance and y_4 is clamp pressure.

4.2.1.2 Modeling of weld width (WW) Based on regression statistics, sequential sum of squares and lack-of-fit tests, it was decided to use a quadratic model for correlation empirical relationship between inputs and outputs. The ANOVA results for finding significant parameters have been presented in Table 10. According to this table, the model Prob > f is lower than 0.05 (i.e. <0.0001) that means the model is significant. Also, the value of Prob > F for term of “lack of fit” is much higher than 0.05 (i.e. 0.1054) that means the “lack of fit” is insignificant. In this table the values of “Prob > F ” <0.0500 indicate model terms are significant and vice versa. Hence the modified model of WW based on significant factors is presented at following equation:

$$\begin{aligned} WW = & 4.01 + 0.26y_1 - 0.37y_2 + 0.59y_3 + 0.058y_4 \\ & - 0.06y_1^2 - 0.2y_3^2 + 0.065y_1y_2 + 0.091y_1y_3 \\ & - 0.2y_2y_3 \end{aligned} \quad (11)$$

where y_1 is laser power, y_2 is welding speed, y_3 is standoff distance and y_4 is clamp pressure.

Table 10 ANOVA results for weld width

Source	Sum of squares	Degree of freedom	Means of squares	F value	Prob > F	Significance
Model	15.44	14	1.1	91.98	<0.0001	Significant
y ₁	1.6	1	1.6	133.57	<0.0001	Significant
y ₂	3.26	1	3.26	271.54	<0.0001	Significant
y ₃	8.4	1	8.4	700.66	<0.0001	Significant
y ₄	0.082	1	0.082	6.81	0.0197	Significant
y ₁ ²	0.1	1	0.1	8.35	0.0112	Significant
y ₂ ²	9.21E-003	1	9.21E-003	0.77	0.3944	Insignificant
y ₃ ²	1.07	1	1.07	89.6	<0.0001	Significant
y ₄ ²	4.57E-003	1	4.57E-003	0.38	0.5460	Insignificant
y ₁ y ₂	0.068	1	0.068	5.64	0.0314	Significant
y ₁ y ₃	0.13	1	0.13	11.11	0.0045	Significant
y ₁ y ₄	2.5E-005	1	2.5E-005	2.08E-003	0.9642	Insignificant
y ₂ y ₃	0.67	1	0.67	56.07	<0.0001	Significant
y ₂ y ₄	2.5E-003	1	2.5E-003	0.21	0.6545	Insignificant
y ₃ y ₄	0.042	1	0.042	3.5	0.0808	Insignificant
Residual	0.18	15	0.012	–	–	
Lack-of-fit	0.16	10	0.016	3.2	0.1054	Insignificant

Table 11 Obtained MAE for various neural network topographies under various data folds for weld strength and Weld width

Structure	Mean absolute error (MAE)					
	Fold #1	Fold #2	Fold #3	Fold #4	Fold #5	Average
Weld strength						
4-3-2	4.7339	4.9233	5.1344	5.2132	5.0112	5.0032
4-4-2	4.2388	4.1654	4.2145	4.5482	4.6211	4.3576
4-5-2	3.7652	3.4322	3.7422	4.0188	4.1422	3.8201
4-6-2	3.2134	3.1138	3.2219	3.4377	3.0145	3.2003
4-7-2	3.9876	3.9877	4.0912	4.2112	3.8973	4.035
4-8-2	4.7652	4.7699	4.8977	4.9823	4.8876	4.8605
Weld width						
4-3-2	0.5543	0.5432	0.5233	0.5643	0.5119	0.5394
4-4-2	0.5214	0.5082	0.4763	0.4873	0.4521	0.4890
4-5-2	0.4632	0.4321	0.4212	0.4123	0.4211	0.42998
4-6-2	0.3801	0.3422	0.3721	0.3892	0.3615	0.3690
4-7-2	0.4532	0.4435	0.4532	0.4877	0.4533	0.4581
4-8-2	0.5893	0.5231	0.5432	0.5689	0.5319	0.55128

The best structure regarding lowest prediction error are in bold

4.2.2 Modeling of weld strength and weld width by ANN

For modeling of weld strength and weld width by neural network, among 30 data sets which were cited in Table 4, numbers of 24 data sets were selected for training of the network and the trained network was tested by the 6 remaining data sets. For purpose of cross validation, five data folds were determined (see “Appendix B”). Table 11 presents values of MAEs for various neural network topographies under different data folds. It is seen from the table that a 4-6-2 topography

ensures lower MAE than other trained/tested architecture. Figure 6 indicates there is tight agreement between measured and predicted values of weld strength and weld width even under the worst prediction (i.e. data fold #4).

4.2.3 Modeling of weld strength and weld width by ANFIS

In order to develop an accurate relationship between laser welding process inputs and responses by ANFIS, among 30 data sets which were cited in Table 4, number of 24 data sets

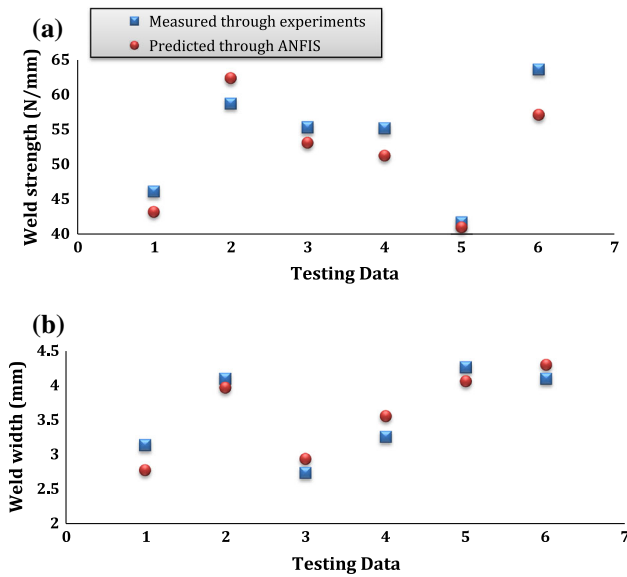


Fig. 6 Comparison of measured and 4-6-2 ANN predicted values of testing data for **a** weld strength, **b** weld width for fold #4

was selected for training of network and the trained network was tested by the 6 remaining data sets. Here, cross validation also performed under 5 data folds (“Appendix B”). Table 12 presents obtained RMSEs under various MFs and different data folds. According to Table 12, it is seen that the 2-2-2-2 ANFIS structure with triangular type of fuzzy membership function guarantees lowest RMSEs for both weld strength and weld width. Figure 7 indicates comparison of measured value of testing data with predicted values obtained through ANFIS for data fold #2. It is seen from the figure that there is tight agreement between measured values and predicted values even for data fold #2 (i.e. worst prediction).

4.2.4 Comparison accuracies of developed models

As discussed earlier, the PEP (Eq. 9) is used for comparison accuracies of developed models. Figure 8 indicates the

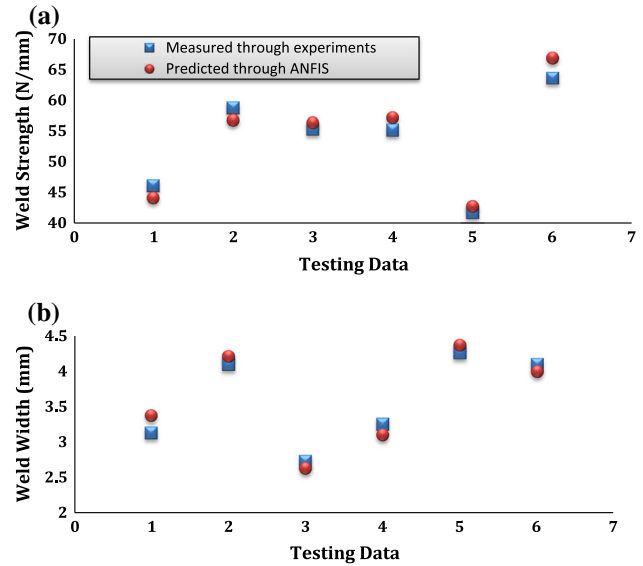


Fig. 7 Comparison of measured and ANFIS predicted values of testing data for **a** weld strength, **b** weld width for fold #2

PEP graph versus all data sets for welding strength and weld width. It is observed from the figure that the developed ANFIS model has lower values of PEP (near to zero) while predicting of laser welding process characteristics. Next to ANFIS, the ANN model has much more precise prediction over RSM. The differences between accuracies of ANFIS and ANN with RSM are very high. The main reason is intelligent nature of ANFIS and ANN while the RSM is a statistical model that is not as precise.

4.2.5 Effect of laser welding parameters on welding strength and welding width based on developed ANFIS model

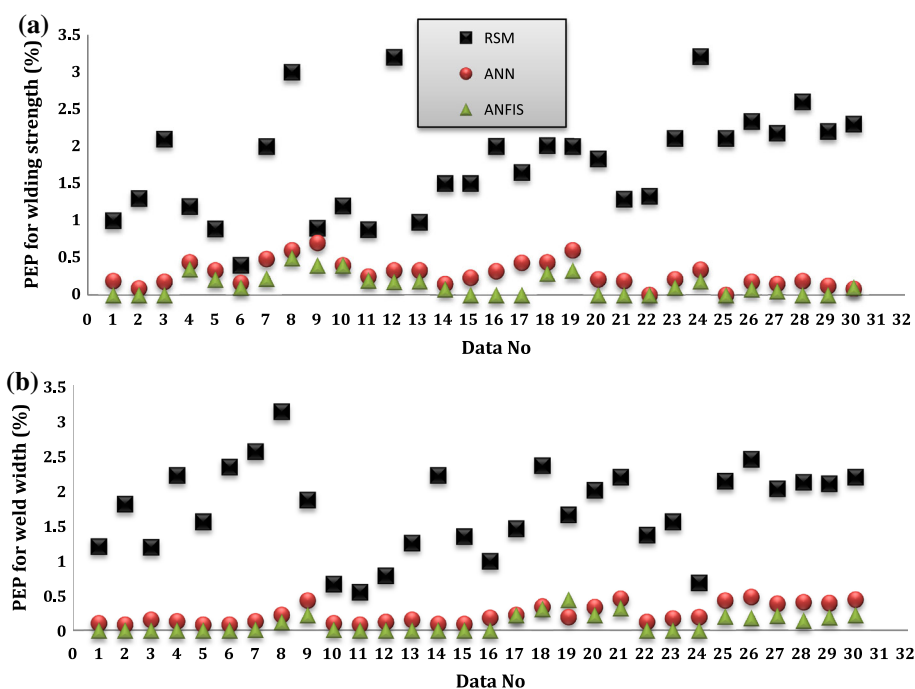
Based on the results, the ANFIS was selected as the most accurate model. Hence, it can be used for analyzing this

Table 12 Obtained RMSEs for various ANFIS MFs under various data folds for weld strength and weld width

Membership functions	Root mean square error (RMSE)					
	Fold #1	Fold #2	Fold #3	Fold #4	Fold #5	Average
Weld strength						
Triangle	1.9831	2.0912	1.7922	1.8314	1.7855	1.8966
Trapezoid	8.2365	10.21	9.1452	7.6541	8.9651	8.8421
Generalized bell	5.6314	6.1966	4.2322	3.5421	4.2365	4.7677
Gaussian	4.6977	4.1821	6.2314	2.6998	4.6541	4.4930
Weld width						
Triangle	0.2154	0.2344	0.2229	0.2019	0.1965	0.2176
Trapezoid	1.0147	1.1221	0.9251	0.8931	0.8569	0.9629
Generalized bell	0.7455	0.8211	0.7169	0.4692	0.4251	0.6355
Gaussian	0.5647	0.6682	0.5589	0.3544	0.3022	0.4896

The best structure regarding lowest prediction error are in bold

Fig. 8 PEP for modeling of **a** welding strength and **b** Welding width by RSM, ANN and ANFIS



process. 3D-surfaces from developed ANFIS models have been plotted to demonstrate interaction effects of laser welding on weld strength and weld width. The discussions about these graphs are presented below.

4.2.5.1 Effect of laser welding parameters on weld strength

Figure 9a and b indicates interaction effects of process parameters on weld strength based on surfaces which were plotted by developed ANFIS models. Formally the higher value of weld strength implies that appropriate welding strategy has been selected. Hence, here, maximal weld strength is desirable.

Figure 9a demonstrates interaction effect of laser power and welding speed on weld strength. For the drawing of this plot the other factors such as standoff distance and clamp pressure were kept constant at their center levels (e.g. 38 mm and 2.1 MPa respectively). It is shown from the figure that high laser power and medium welding speed combination leads to formation of welds with high shear strength. Increase of laser power at medium welding speed results in increase of line energy and hence a good bond is formed; therefore the lap shear strength increases accordingly. At lower welding speed (irrespective to laser power) due to injection of high heat input to weld area, high line energy is formed and may cause to degradation of the base material. While at higher welding speed, low heat input causes to low line energy and it may lead to weak weld due to lack of proper penetration, low heat transfer and low material mixing.

Figure 9b indicates that the clam pressure is not as significant factor as the standoff distance. For the drawing of this plot the other factors such as laser power and welding

speed were kept constant at their center levels (e.g. 15 W and 12 mm/s respectively). Irrespective to clamp pressure, by increasing standoff distance from its initial level to 38 mm the weld strength increases accordingly, but by further increase in standoff distance from 38 to 50 mm the weld strength decreases. On one hand, while the standoff distance increase from the initial level to 38 mm, the laser power energy density increases, and may cause appropriate penetration and proper material mixing. Therefore welds with high strength are formed. On the other hand, by further increasing standoff distance, very high energy density leads to decomposition and degradation of base material. Hence, weld with weak strength are formed while high standoff distance is selected.

4.2.5.2 Effect of welding parameters on weld width

Figure 10a and b indicates interaction effects of process parameters on weld width based on surfaces which were plotted by developed ANFIS models. For prevention of fatigue failure due to stress concentration, lower weld seam width is desirable.

Figure 10a indicates interaction effects of laser power and welding speed on weld seam width. To draw this plot the other factors such as standoff distance and clamp pressure were kept constant at their center levels (e.g. 38 mm and 2.1 MPa respectively). According to this figure, it can be inferred from the figure that higher laser power and lower welding speed combination leads to formation of larger weld seam width. This effect is due to the increase of line energy, which is directly proportional to the laser power and inversely to the welding speed. Hence, by increasing heat input to the weld area, more volume of base materials is welded and resulting larger weld seam width. Therefore, for smaller weld seam

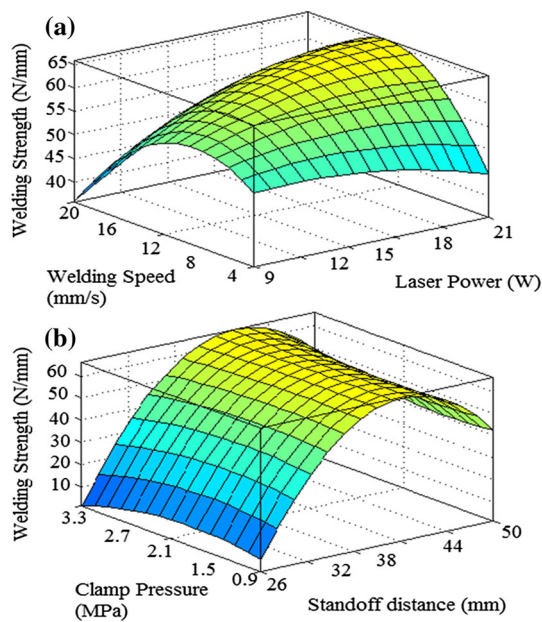


Fig. 9 ANFIS surfaces for interaction effects of parameters on weld strength. **a** Interaction of laser power and welding speed. **b** Interaction of standoff distance and clamp pressure

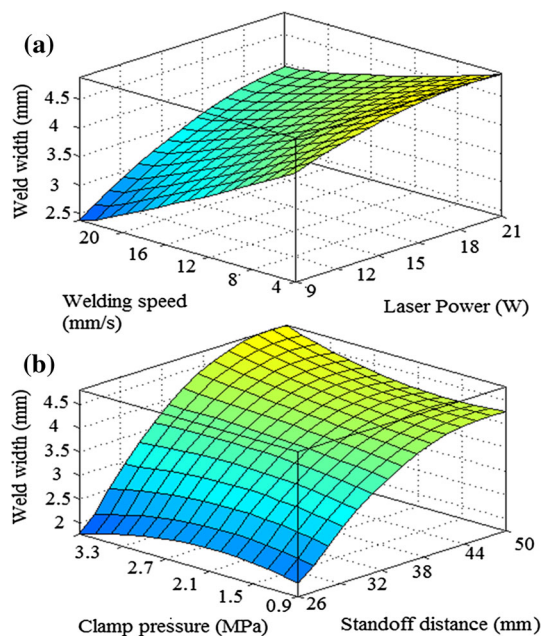


Fig. 10 ANFIS surfaces for interaction effects of parameters on weld seam width. **a** Interaction of laser power and welding speed. **b** Interaction of standoff distance and clamp pressure

width, selection of lower laser power and higher welding speed are suggested.

Figure 10b illustrates interaction effects of standoff distance and clamp pressure on weld width. For the drawing of this plot the other factors such as laser power and welding speed were kept constant at their center levels (e.g. e.g. 15 W

and 12 mm/s respectively). From the figure, it is seen that irrespective to clamp pressure, the weld width increases while the standoff distance increases from 26 to 44 mm and then it becomes almost constant. The main reason is increasing in laser energy density while increasing in standoff distance. At higher energy density higher volume of base material are molten and leads to larger weld seam width.

5 Conclusion

The present work was designed and fulfilled for modeling the characteristics of laser machining and laser welding process via soft computing methodologies. The characteristics of laser machining process were material removal rate and taper of machined holes. Also, the characteristics of laser welding process were lap shear strength and weld seam width. For modeling characteristics of these processes, RSM, artificial neural network (ANN), and ANFIS have been utilized. The accuracy of each model was compared with others based on the prediction error percent. Also, the effect of each process parameters (based on interaction terms) was studied using surfaces which were plotted based on the most accurate model. A summary of obtained results are described as follows:

For laser machining process

1. In modeling of MRR and Ta by RSM, various fitting tests such as sequential model sum of squares, lack-of-fit test and model summary statistics were examined. Results of all fitting tests indicated that the quadratic models with two factor interaction guarantees more accurate prediction than other regression polynomial models.
2. By testing and training of various BPNN architectures, a 5-10-2 network topography was selected as the most accurate architecture due to its lowest value of mean absolute error (MAE) rather than the other trained and tested topographies
3. In modeling of MRR and Ta by ANFIS, the 2-2-2-2-2 ANFIS structure with triangular types of membership function lead to high accuracy prediction for both MRR and Ta.
4. The ANFIS network had the lowest values of error percent among all developed models; hence it was selected as the most accurate model for prediction and analyzing MRR and Ta in laser machining process. Next to ANFIS, the ANN has acceptable accurate prediction while it was compared with RSM.

For laser welding process

1. In modeling of weld strength and weld width by RSM, various fitting tests such as sequential model sum of

squares, lack-of-fit test and model summary statistics were examined. Results of all fitting tests indicated that the quadratic model with two factor interactions guarantees more accurate prediction than other regression polynomial models.

2. A 4-6-2 BPNN architecture was selected as the most accurate topography for prediction of weld strength and weld width by neural network due to its lowest value of MAE which was obtained through trial and error
3. For modeling of weld strength and weld width by ANFIS, various structures with various types of MFs were examined. Finally, it was concluded that for both weld strength and weld width the 2-2-2-2 ANFIS structure with triangular type of MF guarantees more precise prediction.
4. By comparison accuracies of all developed models, the ANFIS was selected as the most accurate predictor due to its lowest PEP. Following ANFIS, ANN has much more precise prediction than RSM.

5.1 Final conclusion

According to the previous sections, it is concluded that the developed ANFIS models have superior predictions for laser machining and laser welding processes. Due to its low values of prediction error percentage, it can be applied as a precise predictor for estimation characteristics of various alternatives of laser manufacturing processes such as laser bending, laser cladding, laser hardening and etc. Due to the fact that the laser materials processing technologies are really expensive, the developed model can give an understanding about selection of appropriate process parameters without needing to a large number of experiments. Otherwise stated, to reach desirable performance in each process, the developed model is beneficial to select optimal parameters without conducting extensive experiments and it has strong economical justification.

Table 13 Splitting of experimental data sets of laser machining process in five folds for implementation of cross validation

No.	Fold #1	Fold #2	Fold #3	Fold #4	Fold #5
1		*			
2			*		
3	*				*
4				*	
5		*			
6			*		
7	*				
8					*
9				*	
10					*
11	*				
12		*			
13			*		
14			*		
15				*	
16		*			
17					*
18					
19	*				
20			*		
21					
22		*			
23				*	
24				*	
25	*				
26					*
27		*			
28			*		
29					*
30	*				
31				*	

Appendix A

See Table 13.

Appendix B

See Table 14.

Table 14 Splitting of experimental data sets of laser welding process in five folds to implement of cross validation

No.	Fold #1	Fold #2	Fold #3	Fold #4	Fold #5
1				*	
2	*				*
3		*			
4				*	
5					*
6	*				
7			*		
8		*			
9				*	
10			*		
11	*				
12				*	
13					*
14		*			
15					
16			*		
17					*
18	*				
19				*	
20		*			
21			*		
22		*			
23	*				
24			*		
25					*
26					
27		*			
28			*		
29	*				*
30				*	

References

- Acherjee B, Misra D, Bose D, Venkadeshwaran K (2009) Prediction of weld strength and seam width for laser transmission welding of thermoplastic using response surface methodology. *Optics Laser Technol* 41:956–967
- Acherjee B, Kuar AS, Mitra S (2012) Experimental investigation on laser transmission welding of PMMA to ABS via response surface modeling. *Optics Laser Technol* 44:1372–1383

- Babajanzade-Roshan S, Behboodi-Jooibari M, Teimouri R, Asgharzade-Ahmadi G, Falahati-Naghbi M, Sohrabpoor H (2013) Optimization of friction stir welding process of AA7075 aluminum alloy to achieve desirable mechanical properties using ANFIS models and simulated annealing algorithm. *Int J Adv Manuf Technol*. doi:10.1007/s00170-013-5131-6
- Choudhury IA, Shirley S (2010) Laser cutting of polymeric materials: an experimental investigation. *Optics Laser Technol* 42:503–508
- Chryssolouris G (1991) *Laser machining: theory and practice*. Springer, Berlin
- Dhupal D, Doloi B, Bhattacharyya B (2009) Modeling and optimization on Nd:YAG laser turned micro-grooving of cylindrical ceramic material. *Optics Lasers Eng* 47:917–925
- Ghosal A, Manna A (2013) Response surface method based optimization of ytterbium fiber laser parameter during machining of Al/Al₂O₃-MMC. *Optics Laser Technol* 47:67–76
- Kashiry Fard R, Azar Afza R, Teimouri R (2013) Experimental investigation, intelligent modeling and multi-characteristics optimization of dry WEDM process of Al-SiC metal matrix composite. *J Manuf Process*. doi:10.1016/j.jmapro.2013.09.002 (in press)
- Kuar AS, Doloi B, Bhattacharyya B (2006) Modeling and analysis of pulsed Nd:YAG laser machining characteristics during micro-drilling of zirconia (ZrO₂). *Int J Mach Tools Manuf* 46:1310
- Onwubolu GC, Davim JP, Oliveira C, Cardoso A (2007) Prediction of clad angle in laser cladding by powder using response surface methodology and scatter search. *Optics Laser Technol* 39:1130–1134
- Shayan AV, Azar Afza R, Teimouri R (2013) Parametric study along with selection of optimal solutions in dry wire cut machining of cemented tungsten carbide (WC-Co). *J Manuf Process*. doi:10.1016/j.jmapro.2013.05.001 (in press)
- Sun Y, Hao M (2012) Statistical analysis and optimization of process parameters in Ti6Al4V laser cladding using Nd:YAG laser. *Optics Lasers Eng* 50:985–995
- Teimouri R, Baseri H (2012a) Artificial evolutionary approaches to produce smoother surface in magnetic abrasive finishing of hardened AISI 52100 steel. *J Mech Sci Technol* 27:533–539
- Teimouri R, Baseri H (2012b) Improvement of dry EDM process characteristics using artificial soft computing methodologies. *Prod Eng Res Dev* 6:493–504. doi:10.1007/s11740-012-0398-2
- Teimouri R, Baseri H (2013a) Forward and backward predictions of the friction stir welding parameters using fuzzy-artificial bee colony-imperialist competitive algorithm systems. *J Intell Manuf*. doi:10.1007/s10845-013-0784-4
- Teimouri R, Baseri H (2013b) Optimization of magnetic field assisted EDM using the continuous ACO algorithm. *Appl Soft Comput*. doi:10.1016/j.asoc.2013.10.006
- Teimouri R, Baseri H, Moharami R (2013) Multi-responses optimization of ultrasonic machining process. *J Intell Manuf*. doi:10.1007/s10845-013-0831-1
- Teimouri R, Baseri H, Rahmani B, Bakhshi-Jooybari M (2012) Modeling and optimization of spring-back in bending process using multiple regression analysis and neural computation. *Int J Mater Forming*. doi:10.1007/s12289-012-1117-4